Figure 2 shows velocity vectors highlighted by the magnitude of streamwise velocity at the hole centerline ($z = 0$). It also shows the interface between the RANS and LES region, where $d_w = C_{\text{des}}\Delta$. It is evident from the figure that the treatment of the initial penetration of jet into freestream is carried out by pure LES technique. This is because of the fine spanwise spacing at the hole exit that switches the code to LES mode.

Figure 3 shows two isosurfaces of x vorticity colored by temperature. The values of the x vorticity for the left and right isosurfaces are $-10{,}000\ \text{s}^{-1}$ and $+10{,}000\ \text{s}^{-1}$, respectively. Light and dark shades of grayscales represent 300 and 150 K, respectively. The injection pipe is shown as reference. It is evident that maximum recirculation is present at the location of initial interaction between the jet and crossflow. The recirculation near the wake region follows a pair of counter-rotating vortices. A sharp temperature gradient is present near the trailing edge of the hole, which becomes more diffused as the flow progresses downstream.

The normalized wall temperature distribution in Fig. 4 indicates that the minimum temperature (0.5) exists at the hole. Downstream maximum cooling takes place in a small area just beyond (less than $1d$) the trailing edge of the hole where the normalized wall temperature is 0.73. In the streamwise direction beginning at approximately $6d$, the normalized temperature reduces to 0.78 and remains cool for nearly $7d$.

Film cooling is a strongly coupled fluid-thermal process. Figure 5 plots the effect of flow structures on normalized fluid temperature on a vertical plane at $x = 3.5d$. The presence of asymmetry is present in the unsteady solution for both velocity vectors and temperature profile. Time-averaged data show prominent features of elongated kidney-shaped bound vortices followed by similar temperature profiles.

Comparison between experimental[1] and numerical (time-averaged DES) values of the centerline and the span-averaged effectiveness is done in Figs. 6a and 6b, respectively. The sharp difference between the experimental[1] and DES time-averaged results for centerline effectiveness at $x = 1d$ stems from the fact that although numerical prediction of maximum cooling occurs near the trailing edge of the hole (similar to the experimental data), its streamwise distribution is very narrow, less than $1d$ (Fig. 4). The experimental and numerical effectiveness follow similar trend between $x = 1d$–$6d$. Beyond $6d$, numerical centerline effectiveness shows higher value than the experimental data, whereas numerical span-averaged effectiveness is lower in that region. Figure 4 clearly shows that there is very little diffusion in the spanwise direction for DES results, which is responsible for the small values of span-averaged effectiveness.

Conclusions

The first detached eddy simulation of film cooling has been presented for a widely published plate-pipe configuration. The blowing ratio was unity and density ratio was two. Results indicate that the mixing processes downstream of the hole are highly anisotropic. DES solution shows its ability to depict the dynamic nature of the flow and capture the asymmetry present in temperature and velocity distributions. Further, comparison between experimental and DES time-averaged effectiveness is satisfactory. Numerical values of centerline and span-averaged effectiveness differ from those of experimental values at downstream locations. Smaller values of numerically predicted spanwise effectiveness than the experimental data might be caused by the improper turbulence model in the spanwise spreading of the jet. This needs to be investigated in the near future.

References

[1]Sinha, A. K., Bogard, D. G., and Crawford, M. E., "Film-Cooling Effectiveness Downstream of a Single Row of Holes with Variable Density Ratio," *Journal of Turbomachinery*, Vol. 113, July 1991, pp. 442–449.

[2]Goldstein, R. J., *Film Cooling, Advances in Heat Transfer*, Vol. 7, Academic Press, New York, 1971, pp. 321–379.

[3]Fric, T. F., and Rosko, A., "Vortical Structure in the Wake of a Transverse Jet," *Journal of Fluid Mechanics*, Vol. 279, 1994, pp. 1–47.

[4]Amer, B., Jubran, A., and Hamdan, M. A., "Comparison of Different Two-Equation Turbulence Models for Prediction of Film Cooling from Two Rows of Holes," *Journal of Numerical Heat Transfer*, Pt. A, Vol. 21, No. 2, 1992, pp. 143–163.

[5]Roy, S., "Numerical Investigation of the Blade Cooling Effect by Multiple Jets Issuing at an Angle," *Journal of Numerical Heat Transfer*, Vol. 38, No. 7, 2000, pp. 701–718.

[6]Garg, V. K., and Rigby, D. L., "Heat Transfer on a Film-Cooled Blade—Effect of Hole Physics," *International Journal of Heat and Fluid Flow*, Vol. 20, No. 1, 1999, pp. 10–25.

[7]Heidmann, J. D., Rigby, D. L., and Ameri, A. A., "A Three-Dimensional Coupled Internal/External Simulation of a Film-Cooled Turbine Vane," *Journal of Turbomachinery*, Vol. 122, No. 2, 2000, pp. 348–359.

[8]Acharya, S., "Large Eddy Simulations and Turbulence Modeling for Film Cooling," NASA CR-1999-209310, 1999, pp. 1–131.

[9]Spalart, P. R., Jou, W. H., Strelets, M., and Allmaras, S. R., "Comments on the Feasibility of LES for Wings, and on a Hybrid RaNS/LES Approach," First AFOSR International Conference on DNS/LES, Air Force Office of Scientific Research, Arlington, VA, 1997.

[10]Strelets, M., "Detached Eddy Simulation of Massively Separated Flows," AIAA Paper 01-0879, Jan. 2001.

[11]Squires, K. D., Forsythe, J. R., Morton, S. A., Strang, W. Z., Wurtzler, K. E., Tomaro, R. F., Grismer, M. J., and Spalart, P. R., "Progress on Detached-Eddy Simulation of Massively Separated Flows," AIAA Paper 02-1021, Jan. 2002.

[12]Grismer, M. J., Strang, W. Z., Tomaro, R. F., and Witzeman, F. C., "Cobalt: A Parallel, Implicit, Unstructured Euler/Navier–Stokes Solver," *Advances in Engineering Software*, Vol. 29, No. 3–6, 1998, pp. 365–373.

[13]Spalart, P. R., and Allmaras, S. R., "A One-Equation Turbulence Model for Aerodynamic Flows," AIAA Paper 92-0439, Jan. 1992.

[14]Kapadia, S., Roy, S., and Wurtzler, K., "Detached Eddy Simulation over a Reference Ahmed Car Model," AIAA Paper 03-0857, Jan. 2003.

[15]Godunov, S. K., "A Difference Scheme for Numerical Computation of Discontinuous Solution of Hydrodynamic Equations," *Matematicheski Sbornik*, Vol. 47, No. 3, 1959, p. 271 (Cornell Aeronautical Lab. translation).

Accelerated Solution of the Radiation-Transfer Equation with Strong Scattering

G. D. Raithby*
University of Waterloo,
Waterloo, Ontario N2L 3G1, Canada
and
E. H. Chui†
National Resources Canada,
Ottawa, Ontario K1A 1M1, Canada

Introduction

THIS Note explains why a method used to accelerate the solution of the radiation-transfer equation (RTE) breaks down, for fine grids, when applied to a purely scattering medium. The explanation is substantiated by showing that a simple strategy can eliminate the problem.

Radiation transfer in a participating medium can be solved in many ways, including the discrete ordinates[1] and the finite volume methods.[2] In these methods the intensities are calculated at discrete nodes in space and for specified directions (or within specified solid angles). For problems involving scattering, the intensity in one direction is usually dependent on the intensities in all other directions. To avoid solving the equations for all directions simultaneously, the

Received 14 January 2003; accepted for publication 19 June 2003. Copyright © 2003 by the American Institute of Aeronautics and Astronautics, Inc. All rights reserved. Copies of this paper may be made for personal or internal use, on condition that the copier pay the $10.00 per-copy fee to the Copyright Clearance Center, Inc., 222 Rosewood Drive, Danvers, MA 01923; include the code 0887-8722/04 $10.00 in correspondence with the CCC.

*Distinguished Professor Emeritus, Department of Mechanical Engineering.

†Senior Research Scientist, CANMET Energy Technology Center.

explicit method is used wherein the intensity in each direction is updated by solving the RTE for that direction with all other intensities taken as temporarily known. To account for the lagged intensities, the equations for intensity in each direction must therefore be solved a number of times, the number depending on the strength of the coupling. For strong scattering convergence can become so slow that the method is practically useless.

The present authors proposed a method for overcoming the problem of slow convergence by solving a separate equation for the average intensity. The original proposal was to use additive correction.[2] Subsequently an implicit method was proposed,[3] which used a multiplicative correction.

Fiveland and Jessee[4] (referred to as F&J) studied various methods of accelerating the solution of the RTE for problems with pure scattering. They concluded that the mesh rebalance method was by far the most successful, at least for coarse spatial grids. They noted that this method, from the neutron transfer literature, was similar to the implicit method of the present authors; it also predated our implicit method by many years. F&J went on to show that the mesh rebalance method breaks down when applied to fine grids.

The breakdown of these acceleration methods is an important issue because they are among the few options available for obtaining economic solutions to problems involving strong scattering. This Note uses the spatial discretization of F&J and focuses on the main problem that led to their observation[4] that the method breaks down.

Application of the Finite Volume Method

Radiation-Transfer Equation

The RTE for intensity I at a given location in the s direction for a gray isotropically scattering medium with scattering coefficient σ is[1]

$$\frac{\partial I}{\partial s} = -\sigma I + \sigma I_a, \qquad I_a = \frac{1}{4\pi}\int_{4\pi} I \, \mathrm{d}\Omega \tag{1}$$

Problem Description

Radiation is to be calculated in an enclosure of dimension $L \times L$ with black walls and with zero intensity entering the enclosure from all but the lower wall. At the lower wall the intensity is unity. All intensities are initialized to 10^{-5}. The objective is to solve for the intensity I and for the average intensity I_a.

Finite Volume Method

The enclosure is subdivided into $M \times M$ square and uniform control volumes of dimension $\Delta = L/M$, of volume V_P, and with a central node P in each volume, as shown in Fig. 1a. This volume interfaces with four neighboring volumes labeled 1, 2, 3, and 4. Direction is divided into L equal solid angles $\Omega^1, \Omega^2 \cdots \Omega^l \cdots \Omega^L$ shown in Fig. 1b. Each solid angle covers the complete range of polar angle $0 \le \phi \le \pi$, where ϕ is measured from the z axis. One intensity I_P^l is associated with each node and each solid angle.

Applying the upwind spatial discretization of F&J, the algebraic approximation of Eq. (1) for the intensity at node P in direction l has the form

$$\left(A_P^l + \sigma V_P \Omega^l\right) I_P^l + \sum_N A_N^l I_N^l = \sigma V_P \Omega^l I_{a,P} \tag{2a}$$

$$I_{a,P} = \sum_l I_P^l \Omega^l \Big/ \sum_l \Omega^l \tag{2b}$$

where N refers to the neighbor nodes of P in Fig. 1a. The coefficients in Eq. (2a) are a special case of those in Ref. 3, where S_f is set to zero.

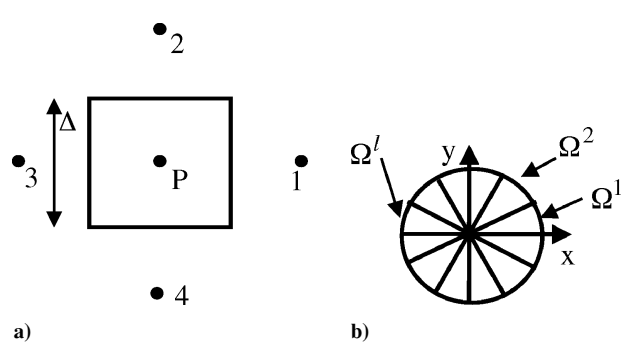

Fig. 1 Control volume in computational mesh and solid angle distribution.

Explicit Method

Applying the explicit method, $I_{a,P}$ is initialized, the intensity is solved for every node for each direction l from Eq. (2a), and the average intensity is then updated from Eq. (2b). This is substituted into the right side of Eq. (2a), and the cycle is continued until convergence is achieved.

Implicit Method

The implicit method attempts to accelerate convergence by improving on the value of $I_{a,P}$ just computed before it is inserted back into Eq. (2a). For clarity, define the values obtained from application of Eqs. (2a) and (2b) as the intermediate values $\tilde{I}_P^l$ and $\tilde{I}_{a,P}$. Phase weights are defined as

$$\alpha_P^l = \tilde{I}_P^l \big/ \tilde{I}_{a,P} \tag{3}$$

To form the new equation for $I_{a,P}$, it is assumed that α_P^l is frozen at this intermediate value, so that the revised (i.e., the end of cycle) values of I_P^l are related to the revised $I_{a,P}$ by

$$I_P^l = \alpha_P^l I_{a,P} \tag{4}$$

Substituting this into Eq. (2a) and summing over all solid angles results in the following equation for $I_{a,P}$. Note that, after summation over l, the scattering term on the left right side of Eq. (2a) has cancelled with the scattering term on the right side.

$$A_P I_{a,P} + \sum_N A_N I_{a,N} = 0, \tag{5}$$

where

$$A_P = \sum_l A_P^l \alpha_P^l, \qquad A_N = \sum_l A_N^l \alpha_N^l$$

The solution cycle is now modified by updating the value of $I_{a,P}$ using Eq. (5) before it is inserted into Eq. (2a) at the top of the cycle.

Convergence Criterion for Cycle

The residual of Eq. (5) is defined as

$$R_P = \frac{A_P I_{a,P} + \sum_N A_N I_{a,N}}{A_P Rng(I_{a,P})}, \qquad R_{\max} = (R_P)_{\max} \tag{6}$$

where $Rng(I_{a,P})$ is the range of $I_{a,P}$ in the problem and $R_{\max}$ is the maximum residual. The maximum residual on the first cycle is $R_{\max}^0$. When either the explicit or implicit method is used, the values of I_a used in Eq. (6) are those from the solution of Eq. (2). [To be strictly consistent with the nomenclature just introduced, I_a in Eq. (6) should be replaced by $\tilde{I}_a$ when the implicit method is used.] The solution cycle was continued in the present study until $R_{\max}/R_{\max}^0 \le 10^{-4}$ was achieved or a maximum cycle count was exceeded.

Solution of the Linear Equations

A point-Gauss–Seidel solver was used to solve Eqs. (2) and (5). One iteration is defined as one application of the solver over all possible Cartesian sweep patterns. Because of the parabolic character of Eq. (2), one iteration achieves the solution to within roundoff. Iteration on Eq. (5) was continued until a residual of 10^{-6} was achieved or until an upper bound of 100 iterations was reached. This extremely tight tolerance was adopted to ensure that the observed results were not contaminated by a failure to drive the linear equation sets to convergence.

Results

Results are presented for a suite of problems with $M \times M$ grids ($M = 5, 10, 25, 50, 100$), and for 24 equal solid angles, and for values of σ to give cell optical thicknesses in the range $0.001 < \sigma\Delta < 100$.

Explicit Method

Results from application of the explicit method, with an upper bound of 2000 cycles, are presented in Table 1. When convergence was not achieved, the residual reached on the last cycle was recorded, and a bar drawn across the cell. The method becomes impractical for large values of $\sigma M \Delta$. These results provide a baseline for comparison with the implicit method.

Implicit Method

Results for the same suite of problems are presented in Table 2. In eight cases (the cells with bars) for fine grids and $0.07 \le \sigma\Delta \le 1.0$, convergence was not achieved. In fact the code diverged for three of these cases, as indicated by "Div" in a cell. In cases where residuals are recorded, the residuals decreased to roughly the levels shown, and then bounced. Allowing more cycles did not result in convergence. For coarse grids the method works well for all values of $\sigma\Delta$, as originally reported[3] and as verified by F&J. Not shown on the table, but of practical importance, is the observation that the iterative solution of Eq. (5) did not always achieve the target residual of 10^{-6} within the limit of 100 iterations. This was costly in terms of CPU time; the reason is given next.

Understanding the Performance of the Implicit Method

First, to explain the reason for poor convergence when the iterative solver is applied to Eq. (5), it is observed that diagonal dominance (i.e., $A_P + \sum_N A_N \ge 0$) is not guaranteed at all nodes. The coefficient sum becomes negative in regions of the grid where α_P^l changes quickly between nodes. This can lead to wiggles in the solution to the equation. It also degrades the performance of the iterative solver.

The poor convergence of the iteration cycle, indicated in Table 2, is now discussed. The interactions between equations that must cause this behavior cannot be a very complex because there are only two: 1) The calculated values of $I_{a,P}$ from Eq. (5) are influenced by the I_P^l values from the solution of Eq. (2a) only through the phase weights α_P^l. 2) The calculated values of I_P^l from Eq. (2a) are influenced by the$I_{a,P}$ values computed from Eq. (5) only through the term on the right-hand side. To obtain rapid convergence, it is necessary that at least one of these influences be weak.

For $\sigma\Delta \gg 1$ scattering is so dominant that the I_p^l intensities from Eq. (2a) are very nearly isotropic. Because the information that flows from Eq. (2a) to Eq. (5) (i.e., α_P^l values close to unity) is almost independent from the information that flows back from Eq. (5) to Eq. (2a), convergence is achieved after a few cycles. For $\sigma\Delta \ll 1$ the term on the right side of Eq. (2a) is small, independent of the exact values of $I_{a,P}$ because σ is small. Hence the linkage between Eq. (5) and Eq. (2a) is weak, and rapid convergence is again observed.

For intermediate $\sigma\Delta$ the phase weights on a given cycle can be asymmetric, being larger in directions pointing away from the lower surface. This results in asymmetric coefficients A_N in the $I_{a,P}$ equation, with those on the lower side of node P being larger. This causes an increase in the level of $I_{a,P}$ in the enclosure, which when inserted into Eq. (2a) yields I_P^l values that are more isotropic (the phase weights are more symmetric), which then reduces the interior values of $I_{a,P}$, etc. The residuals bounce from cycle to cycle about some level in a chaotic manner. No oscillations appear on a coarse grid, presumably because the number of degrees of freedom is too small.

The lack of diagonal dominance in the $I_{a,P}$ equation appears to amplify the resonance between the equations. This was checked by introducing relaxation into Eq. (5) to ensure that $A_P + \sum_N A_N \ge 0$. [Equation (7) was used with $\varepsilon^* = 0$.] This eliminated all cases of divergence indicated in Table 2, but the residuals still bounced, and convergence was not achieved.

Introduction of Relaxation

If the explanation just given is correct, it should be possible to promote convergence by damping the interactions between equations. Equation (5) was modified to

$$A_P(1+\varepsilon)I_{a,P} + \sum_N A_N I_{a,N} = \varepsilon A_P \tilde{I}_{a,P} \tag{7}$$

where

$$\varepsilon = \max\left[\varepsilon^* - \frac{\left(A_P + \sum A_N\right)}{A_P}, 0\right]$$

and Eq. (3) was underrelaxed as follows:

$$\alpha_P^l = (1-\omega)\tilde{I}_P^l \Big/ \tilde{I}_{a,P} + \omega\left(\alpha_P^l\right)^{old} \tag{8}$$

The superscript *old* refers to the earlier calculated value of α_P^l.

The following simple strategy was implemented. Before the solution was begun, the values of ω and ε^* were initialized to zero. If the maximum residual $R_{\max}$ did not reduce by at least a factor of two on any given cycle, then ω was incremented by 0.1, and

Table 1 Cycle count to achieve convergence for the explicit method (Cells show residuals when convergence was not achieved in 2000 cycles)

	$\sigma\Delta$								
Grid	0.001	0.01	0.07	0.10	0.30	0.50	1.0	10	100
5×5	2	3	6	7	14	22	44	540	~~1×10^{-4}~~
10×10	2	3	7	9	25	44	102	1478	~~4×10^{-2}~~
25×25	2	4	13	19	71	144	375	~~3×10^{-2}~~	~~5×10^{-2}~~
50×50	2	5	24	38	182	388	1042	~~5×10^{-2}~~	~~5×10^{-2}~~
100×100	2	7	54	90	480	1024	~~2×10^{-4}~~	~~5×10^{-2}~~	~~5×10^{-2}~~

Table 2 Cycle count to achieve convergence for the implicit method (Cells show residuals when convergence was not achieved in 150 cycles)

	$\sigma\Delta$								
Grid	0.001	0.01	0.07	0.10	0.30	0.50	1.0	10	100
5×5	2	3	4	5	7	8	8	5	4
10×10	2	3	5	6	10	12	11	6	4
25×25	2	3	9	12	79	60	23	6	4
50×50	2	4	31	~~3×10^{-2}~~	~~2×10^{-2}~~	~~2×10^{-2}~~	61	6	4
100×100	2	5	~~7×10^{-1}~~	~~7×10^{-2}~~	Div[a]	Div	Div	8	8

[a]Divergence.

Table 3 Cycle count to achieve convergence for the implicit method with relaxation

	$\sigma\Delta$								
Grid	0.001	0.01	0.07	0.10	0.30	0.50	1.0	10	100
5×5	2	3	4	5	7	7	8	5	4
10×10	2	3	5	6	10	10	11	5	4
25×25	2	3	9	11	15	13	11	5	4
50×50	2	4	15	16	14	13	11	5	4
100×100	2	5	14	15	21	14	12	6	5

ε^* was incremented by 0.0025, provided that upper bounds on ω and ε^* are not exceeded. The upper bounds were set at 0.4 and $0.025/(1+\sigma\Delta)$, respectively. No attempt was made to optimize the procedure.

Results with Relaxation

The results in Table 3 were obtained using this relaxation strategy. Rapid convergence was achieved for all cases. In addition, the cost of solving Eq. (5) for $I_{a,P}$ was reduced because fewer solver iterations were required.

Conclusions

A strong two-way coupling between the equations or directional intensity I_P^L and the equation for the average intensity $I_{a,P}$ exists for intermediate scattering strengths ($0.1 \leq \sigma\Delta \leq 1.0$). This slows or prevents convergence for fine grids. Damping of the interequation couplings is needed to achieve rapid convergence. Rapid convergence is achieved on coarse grids for all $\sigma\Delta$, presumably because of the reduced number of degrees of freedom.

Acknowledgment

This research was sponsored by the Natural Sciences and Engineering Council of Canada.

References

[1]Fiveland, W. A., "Three-Dimensional Radiative Heat-Transfer Solutions by the Discrete Ordinate Method," *Journal of Thermophysics and Heat Transfer*, Vol. 2, No. 4, 1998, pp. 309–316.

[2]Raithby, G. D., and Chui, E. H., "A Finite Volume Method For Predicting Radiant Heat Transfer in Enclosures with Participating Media," *Journal of Heat Transfer*, Vol. 112, 1990, pp. 415–423.

[3]Chui, E. H., and Raithby, G. D., "An Implicit Solution Scheme to Improve Convergence Rate in Radiative Transfer Problems," *Numerical Heat Transfer*, Pt. B, Vol. 22, No. 3, 1992, pp. 251–272.

[4]Fiveland, W. A., and Jessee, J. P., "Acceleration Schemes for the Discrete Ordinate Method," *Journal of Thermophysics and Heat Transfer*, Vol. 10, No. 3, 1996, pp. 445–451.